Chapter 6
Experimental and Numerical Analysis of Dynamic Behavior of Cork Material

Veronica Ilari, Carlo Sabbatini, and Marco Sasso

Abstract In this research, the agglomerated cork material is considered for energy absorption purposes. Indeed, the stress-strain curve of cork describes the distinctive mechanical behavior of cellular materials: it can withstand large deformations under compression loading with a smooth transition from elastic to plateau region, and then from plateau to densification stage. In order to characterize the visco-hyperelastic behavior, compression tests have been conducted at different strain rates on cork samples. Low and intermediate strain rate tests have been carried out by means of standard electromechanical and pneumatic testing machines, whereas high strain rates have been carried out using a split Hopkinson pressure bar. The compression tests have been extended including the unloading stage, where the load is progressively removed; in this way, it was also possible to describe the damage evolution within the material according to the Mullins effect theory, which has been borrowed here from the literature on rubber-like materials. It was implicitly assumed that the same behavior occurs in dynamic conditions. The energy absorption capability of a shock absorber made of cork can be evaluated by means of puncture tests that are typically conducted using drop tower rigs. Such tests have been numerically reproduced in Abaqus/Explicit software, where the main features of the material behavior have been included by developing user defined subroutines. The punch deceleration peak and rebound speed, together with the residual deformation and damage of the cork absorber, have been analyzed as performance parameters.

Keywords Cork · Strain rate · Energy absorption · Hyperelasticity · Viscoelasticity

Introduction

In the last decades, cellular materials have been used in various engineering applications, particularly where high energy absorption capability is required. These materials are also valued for their damping and isolation properties, making them essential in impact protection systems. As a result, they are commonly employed in crash test devices designed for personal safety (such as in road accident, where these materials are used for the production of motorcycle helmets) and for protection of things/products (such as in packaging) [1] [2].

Cork is a natural material that is obtained from the outer bark of the cork oak (*Quercus suber*). It has a cellular structure with small closed cells (4-20 x 107 cels/cm^3) that form a highly ordered honeycomb pattern, a characteristic that stems from its biological formation process. Cork shows an interesting set of properties, including low values of density, permeability and energy transfer coefficients with a remarkable elastic behavior and high physical, chemical and biological stability [3].

When subjected to compression, cellular materials like cork can suffer a large deformation, maintaining relatively constant stress levels until densification occurs. This behavior allows them to absorb large amounts of energy. The stress-strain curve of cork exhibits three distinct phases: an initial linear elastic phase at low stresses, primarily governed by the bending of cell walls; a long plateau region, where the material undergoes progressive collapse while dissipating energy through structural deformation; and a densification phase, in which the stress rises sharply due to the complete compaction of the cellular structure [4] [5].

Veronica Ilari · Carlo Sabbatini · Marco Sasso
Dipartimento di Ingegneria Industriale e Scienze Matematiche
Università Politecnica delle Marche, 60131, Ancona, Italy
e-mail: m.sasso@univpm.it; c.sabbatini@pm.univpm.it; v.ilari@pm.univpm.it

Karen Kasza et al. (eds.), *Mechanics of Biological Systems and Materials and the Mechanics of Composite, Hybrid & Multifunctional Materials, Vol. 3*, Conference Proceedings of the Society for Experimental Mechanics Series, https://doi.org/10.13052/97887-438-0829-9_6

Beyond its energy absorption capability, cork also possesses a remarkable recovery capacity. This means that its deformation is mostly elastic, allowing it to return to its original shape once the load is removed. This characteristic is particularly advantageous, because it allows the material to maintain its energy absorbing capacity almost unchanged, even after repeated impacts [6] [7].

To characterize the visco-hyperelastic behavior of cork, quasi-static and dynamic compression tests were carry out with a strain rate between 10^{-3} and 10^{3} s^{-1}. The resulting stress-strain curves were used to calibrate the constitutive model parameters that describe cork's mechanical response. In particular, the hyperelastic behavior was modeled by the Ogden hyperfoam formulation; while viscoelasticity was described through a Prony series model (generalized Maxwell model). Additionally, the unloading phase was analyzed to evaluate damage evolution of the material and the potential release of stored elastic energy that can occurre after the impact. The Mullis effect was incorporated to describe the unloading phase [8].

To validate the proposed constitutive model, numerical simulations were performed using the finite element Abaqus/Explicit software. The experimental compression tests were reproduced in the simulation environment, integrating the material properties through user-defined subroutine (VUMAT).

Finally, the energy absorption performance of a cork based shock absorber was evaluated through puncture tests, conducted using a drop tower. These tests were numerically reproduced in Abaqus/Explicit software. The comparison between numerical and experimental results serves as a crucial validation step, ensuring the model's accuracy in predicting the mechanical response of cork under different loading conditions.

Materials and Methods

Compression tests were performed on agglomerate cork samples (Fig.1a) with a base size of 12 x 12 mm and a height of 15 mm. They have a density of 140 kg/m^3. Tests with a strain rate of 10^{-3}, 10^{-1} and 10^{1} s^{-1} were conducted through a servo-pneumatic machine model Siplan® (Fig.1b), equipped with a 3 kN load cell and capable of reaching a piston speed of 100 mm/s, while dynamic tests with a 10^{3} s^{-1} strain rate were performed with a Split Hopkinson Pressure bar (SHPB).

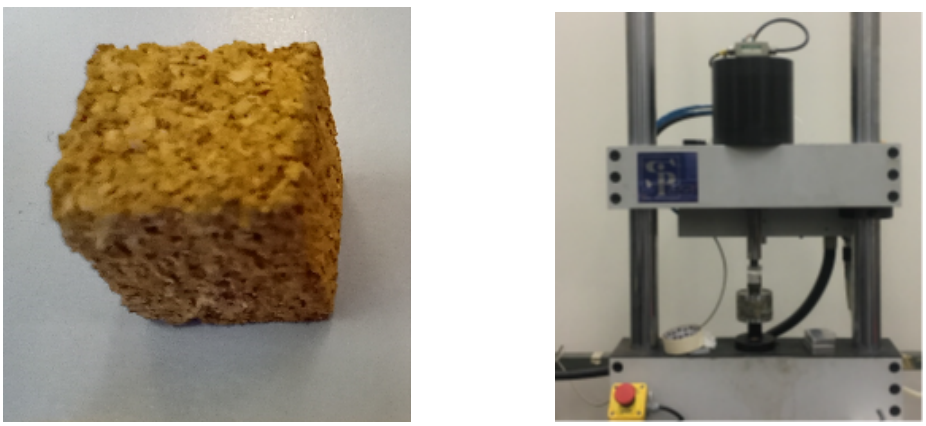

(a) (b)

Fig. 1 a) Agglomerated cork sample; b) Servo-pneumatic testing machine

For the tests conducted at 10^{-3} and 10^{-1} s^{-1}, the samples were placed on a flat plate connected to the load cell, located on the fixed crosshead of the machine. The piston was then moved with precision, until it touches the upper surface of the sample, marking the start of the test.

For the tests conducted ad 10^{1} s^{-1}, however, the piston was initially raised to a sufficient distance from the sample, allowing it to complete the acceleration phase from zero to a 100 mm/s velocity. This strategy allowed to keep the deformation of the samples as uniform as possible, compatible with the capabilities of the machine. To analyze the relaxation phase of the material in tests with 10^{-3} and 10^{-1} s^{-1} strain rate, the deformation was manteined unchanged at the end of the loading ramp for a period equal to the duration of the ramp itself. Subsequently, the load was progressively reduced by moving the piston backwards until the applied load is completely removed.

Dynamic test at 10^{3} s^{-1} strain rate were performed using a Split Hopkinson Pressure Bar (SHPB), shown in Fig.2. The calibration and the fitting of this system for the study of soft materials are described in [9] [10]. Furthermore, the SHPB

Fig. 2 Split Hopkinson Pressure Bar installed at Marche Polytechnic University

configuration allowed a partial valutation of the relaxation of the sample, extending the analysis of reflected and transmitted waves. This made it possible to partially measure the unloading phase after reaching the maximum load, without a holding phase [11].

Material Modelling

Constitutive models

The constitutive models that describe the material were defined using a VUMAT, that is a user defined subroutine implemented in Abaqus/Explicit.

In this analysis, the agglomerated cork is mainly modeled as a hyperelastic material, using the Ogden hyperfoam model. It is a non linear model, usually used to characterize elastomeric foams that exhibit hyperelastic behavior. It is also intended for finite strain applications where the material can deform elastically to large strains, up to 90 % strain in compression. This model is based on a strain energy potential W. This model is implemented as a built-in material within the Abaqus FE commercial code as "Hyperfoam". The strain energy function of order N is defined:

$$W = \sum_{1=1}^{N} \frac{2\mu_i}{\alpha_i^2} \left[\lambda_1^{\alpha_i} + \lambda_2^{\alpha_i} + \lambda_3^{\alpha_i} - 3 + \frac{1}{\beta_i}(J^{-\alpha_i \beta_i}) \right] \tag{1}$$

where μ_i, α_i and β_i are material constants, $\lambda_{1,2,3}$ are the stretch ratios in the three principal directions, and J is the volume ratio, $J = \lambda_1 \lambda_2 \lambda_3$. The principal stresses are computed taking the partial derivative of Eq.(1) with respect to λ. The experiments also highlighted that cork has a Poisson's ratio of almost zero, thus making the use of a compressible hyperelastic model more appropriate. The μ_i coefficient is directly correlated to the initial shear modulus G, while β_i is related to Poisson's ratio, ν_i, by the expressions:

$$G = \sum_{i=1}^{N} \mu_i \qquad\qquad \nu_i = \frac{\beta_i}{1 + 2\beta_i} \tag{2}$$

Therefore, the null Poisson's ratio determines that $\beta_i = 0$. In uniaxial case $\lambda_2 = \lambda_3 = 1$, the principal stresses are obtained from:

$$\sigma = \frac{\partial W}{\partial \lambda_1} = \sum_{1=1}^{N} \frac{2\mu_i}{\alpha_i \lambda_1} (\lambda_1^{\alpha_i} - 1) \tag{3}$$

The Eq.(3) is used to fit the best parameters of the model using the quasi-static compression curve [12].
The agglomerate cork shows a viscoelastic behavior that emerges in dynamic load conditions. Consequently, the viscoelastic behavior must also be modeled in conjunction with the hyperelastic model. The Prony series (or generalized Maxwell) model was chosen. This model considers the material as a branch with a spring representing the long-term stiffness G_∞, in parallel with a series of N_G Maxwell branches, where a spring and a viscous damper are present. Each Maxwell branch is characterized by a relaxation time τ_i. The global relaxation modulus of such a system is given by:

$$G(t) = G_0 \left[g_\infty + \sum_{i=1}^{N_G} \left(g_i e^{-t/\tau_i} \right) \right] \tag{4}$$

In Eq.(4), g_i are the relative moduli, so that $g_\infty + \sum g_i = 1$; G_0 represents the short term, or instantaneous, stiffness that is obtained as the sum of all branches' stiffness. The long term and short term stiffnesses are related as $G_\infty = g_\infty \cdot G_0$. The stress along time in the i-th layer of the Generalized Maxwell model is given by:

$$(\mathbf{S}_i^{2d})_{n+1} = exp\left(-\frac{\Delta t}{\tau_i^G}\right)(\mathbf{S}_i^{2d})_n + \alpha_i^G exp\left(-\frac{\Delta t}{2\tau_i^G}\right)\left[\frac{d\Phi}{d\mathbf{C}_{n+1}} - \frac{d\Phi}{d\mathbf{C}_n}\right] \tag{5}$$

where $\mathbf{S}_i^{2d}$ is the second Piola-Kirchhoff stress tensor and $\mathbf{C}$ is the right Cauchy-Green deformation tensor. The true stress can be obtained from:

$$\sigma = \frac{2\mathbf{F}\mathbf{S}^{2d}\mathbf{F}^T}{J} \tag{6}$$

where $\mathbf{F}$ is the deformation gradient [13].

The total stress can be obtained from the sum of the hyperleastic stress with the N_G viscoelastic stresses.

In order to correctly model permanent energy dissipation effects and stress softening in agglomerate cork, Mullins effect is implemented, providing an extension to the elastomeric foam model [14]. Therefore, this damage model is used to include the damage present in elastomeric foams, modeling the energy absorption in foam components subjected to dynamic loading, with high strain rates compared to the characteristic relaxation time of the foam. In this model, energy dissipation effects are considered by introducing an augmented strain energy density function of the shape:

$$W(\lambda_i, \eta) = \eta W(\lambda_i) + \phi(\eta) \tag{7}$$

The function $W(\lambda_i, \eta)$ is a continuous function of the damage variable, η, and is related to the damage function $\phi(\eta)$. The damage variable, η, varies continuously during the course of deformation and always satisfies $0 < \eta < 1$, with $\eta = 1$ at the points of the primary curve (described by the Hyperfoam model). Taking into account the Mullins effect, the stresses are calculated by:

$$\sigma(\lambda_i, \eta) = \eta\sigma(\lambda_i) \tag{8}$$

where $\sigma(\lambda_i)$ is the stress corresponding to the primary behavior of the foam at the current strain level λ_i. Then, the stress is obtained by simply scaling the stress of the primary behavior of the foam by the damage variable η. Eq.8 is used when the material is at an energy potential W that is lower than the maximum energy potential W_m experienced by the material itself at the end of the loading phase. The damage variable is generally assumed to be represented by the so called "error function":

$$\eta = 1 - \frac{1}{r} erf\left(\frac{W_m - W}{m + \beta W_m}\right) \tag{9}$$

where r,m and β are material parameters that govern the shape of the unloading curve. Note that $r > 1$, $m \geq 0$, $\beta > 0$ [15].

Validation

In order to obtain the coefficients of the models used to describe the cork behavior, an optimization technique was implemented. Specially, a cost function, which represents the difference between the experimentally obtained stresses and those predicted analytically, is minimized.

To describe the compressible hyperelastic behavior, a fourth-order Hyperfoam model was adopted, which requires the identification of 8 parameters, namely the coefficients μ_i and α_i with $i = 1 \ldots 4$.

The viscoelastic behavior was instead modeled by a 10-term Prony series, where the Maxwell branches have relaxation times uniformly distributed on a logarithmic scale. Consequently, the optimization problem focuses on the determination of the two extreme relaxation times τ_{min} and τ_{max} and the 10 related moduli g_i. Lastly, Mullins effect requires the calibration of three parameters r,m and β. The optimization process was implemented in Matlab. All the optimized parameters are listed in Table 1, 2 and 3 for the Ogden hyperfoam model, Prony series model and Mullins damage, respectively.

Table 1 4^{th} order Ogden hyperfoam parameters

μ_1	α_1	μ_2	α_2	μ_3	α_3	μ_4	α_4	$\beta_{1\cdots4}$
4.236	7.532	-5.579	5.580	2.543	4.146	0.007	-3.137	0

After material model calibration, the impact tests were simulated by means of the commercial Finite Element software. In particular, the Abaqus/Explicit code was adopted because it is well suited for implementing user-defined constitutive models by means of user-defined Fortran subroutines (VUMAT).

Table 2 Prony series with 10 terms parameters

τ_{min}	τ_{max}	g_1	g_2	g_3	g_4	g_5	g_6	g_7	g_8	g_9	g_{10}	g_∞
1E-5.608	1E1.322	0.140	0.703	0.046	0.023	0.012	0.006	0.007	0.009	0.006	0.005	0.042

Table 3 Mullins damage parameters

r	m	β
1.067	0.740	0.628

Compression tests were performed at different strain rates on cork block, in order to reproduce as faithfully as possible the experimental tests. The cork is modeled as a 2D model costrained to the bottom side. The plate that load the cork is discretized as a rigid surface and a constant velocity equal to the experimental values. The strain rate analyzed are 10^{-3}, 10^{-1}, 10^{1}, and 10^{3} s^{-1}. The results of both the experimental tests and the analytical modeling, expressed in terms of stress-strain curves, are shown in Fig.3a and in Fig.3b. The blue curves represent the experimental points, while the curves in red represents the total stress predicted by the constitutive model.

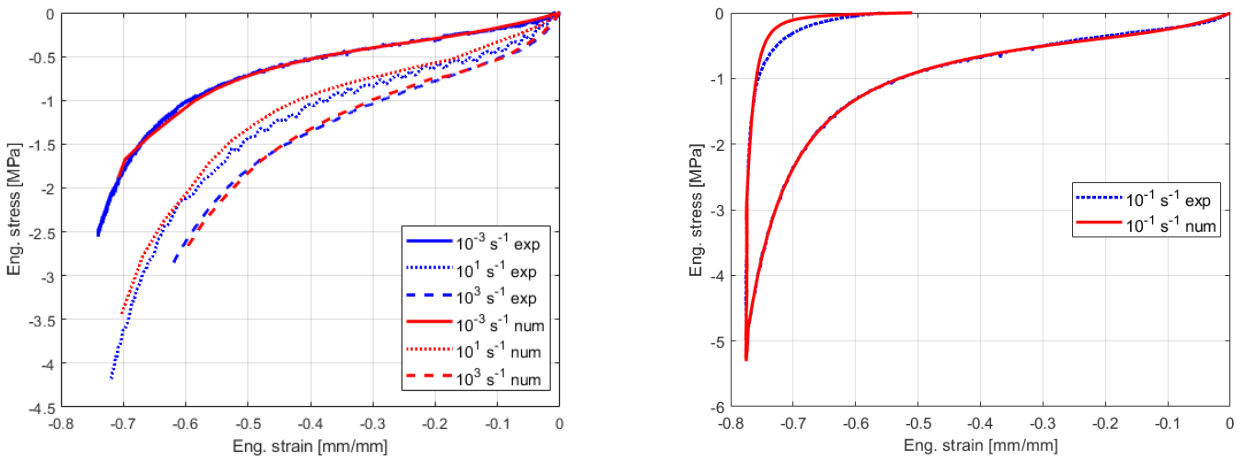

(a) (b)

Fig. 3 a) Compression stress strain curves at 10^{-3}, 10^{1} and 10^{3} s^{-1} strain rate; b) Compression stress strain curves at 10^{-1} s^{-1} strain rate

The Fig.3a presents the results for the compression tests at 10^{-3}, 10^{1} and 10^{3} s^{-1}. The stress-strain curve at the lowest strain rate validates the hyperelastic model, while the two curves corresponding to the highest strain rates confirm the accuracy of the viscoelastic model.

The Fig.3b illustrates the validation of the complete model, including damage, which is captured through the Mullins effect. This test was performed at a strain rate of 10^{-1} s^{-1}.

Test Case

In the previous sections, we defined the constitutive models that best describe the behavior of agglomerated cork. We then validated the model through the simulation of an impact test at different strain rates.

In this section, we present a test case: puncture tests performed using a hemispherical rigid indenter. Puncture tests were performed on cylidrical slabs of cork by means of a drop tower machine. This kind of test is very popular as it provides immediate information on the energy absorption. However, here it has been used for verifying the material models calibration. The specimen is placed between two supports with a 40 mm hole, and is deformed by a falling punch having a

hemispherical impact head of 12.7 mm diameter. The speed of the punch is measured by an optical sensor. This test serves as an additional validation step, assessing the model's ability to predict material response under localized loading conditions.

The tests were performed at two different velocities: 0.79 m/s and 1.27 m/s.

The puncture tests have been replicated numerically by means of the FE model and material subroutine VUMAT. The finite element model was developed to closely replicate the experimental setup, ensuring consistency in boundary conditions and loading conditions. A 2D axisymmetric model of the cork block and the impacted area, along with the impactor, was created. The cork block is meshed with 2D axisymmetric reduced integration elements (CAX4R) [16]. The impactor is discretized as a rigid shell, with a 3.055 kg mass and an initial velocity equal to the experimental values. The cork was laterally constrained, as in the experimental test.

Material properties obtained from the previous calibration were assigned to the numerical model, incorporating both hyperelastic and viscoelastic behavior, as well as Mullins damage effects.

The results of the finite element simulations for the puncture tests at impact velocities of 0.79 m/s and 1.27 m/s are presented in Fig.4 and Fig.5, respectively. These contour maps illustrate the distribution of logarithmic strain at three key stages of the impact event: (a) the initial contact between the indenter and the cork specimen, (b) the moment of maximum penetration, and (c) after rebound, when partial recovery of the deformation occurs.

At the instant of maximum penetration (Fig.4b and Fig.5b), it is evident that the deformation in the case of the higher impact velocity (1.27 m/s) is significantly greater than in the lower velocity case (0.79 m/s). The strain distribution in Fig.5b shows a more concentrated and intense deformation region beneath the indenter, indicating a stronger material response to the higher loading rate. This suggests that at increased impact velocities, the cork undergoes greater compression and energy absorption before rebound.

Fig.4c and 5c shows the partial recovery of the strain that occurs when the impact rebounds. It can be seen that the indentation left by the impact is less pronounced in Fig.4c than in Fig.5c and the logarithmic strain is reduced.

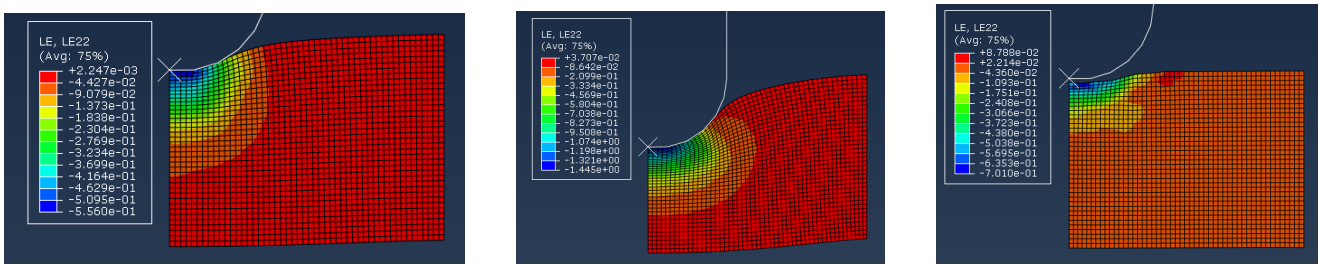

(a) (b) (c)

Fig. 4 Contour maps of logarithmic strain from FE simulations of impact tests at 0.79 m/s a) at the beginning; b) at the instant of maximum penetration; c) after rebound

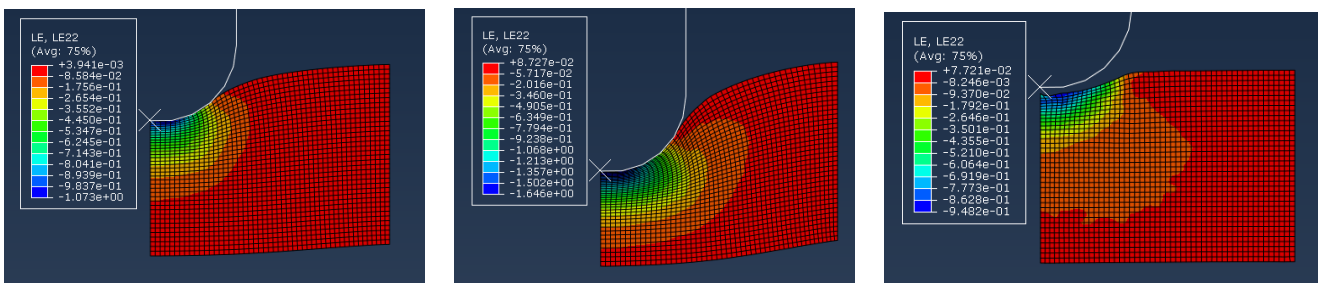

(a) (b) (c)

Fig. 5 Contour maps of logarithmic strain from FE simulations of impact tests at 1.27 m/s a) at the beginning; b) at the instant of maximum penetration; c) after rebound

Conclusion

In this work, we have presented the mechanical characterization and constitutive modelling of agglomerated cork subjected to compression loading. The compression stress-strain curves exhibit the typical behavior of cellular materials. Constitutive models incorporating hyperelasticity, viscoelasticity and the Mullins damage effect were developed and calibrated. These models were then validated through numerical simulations using a VUMAT subroutine, which aimed to accurately reproduce compression tests at different strain rates and provide a comprehensive description of the material's dynamic behavior.

To further assess the constitutive model under more complex loading conditions, we conducted a puncture test at two different impact velocities: 0.79 m/s and 1.27 m/s. The experimental and numerical approaches were integrated to validate the material models, ensuring they accurately capture the complex response of cork under impact loading.

These results confirm that the proposed material models are capable of accurately predicting the cork's behavior under dynamic loading conditions. This validation makes the models a valuable tool for future research on agglomerated cork and similar materials, offering insights into the material's performance in energy absorbing applications and impact resistant designs.

The successful validation of the cork material model through these puncture tests not only reinforces its relevance for practical applications but also provides a solid foundation for future studies.

References

1. Fernandes, F.A.O., Sousa, R.J.A.D., and Pascoal, R.J.S. "Modelling impact response of agglomerated cork". *Materials & Design*, 58:499–507 (2014)
2. Utzeri, M., Cebeci, H., and Kumar, S. "Autonomous sensing architected materials". *Advanced Functional Materials*, 2411975 (2024)
3. Pereira, H. "The rationale behind cork properties: A review of structure and chemistry". *BioResources*, 10 (2015)
4. Anjos, O., Pereira, H., and Rosa, M.E. "Tensile properties of cork in axial stress and influence of porosity, density, quality and radial position in the plank". *Eur. J. Wood Prod.*, 69:85–91 (2011)
5. Gibson, L.J. and Ashby, M.F. *Cellular Solids: Structure and Properties. 2nd ed.* Cambridge University Press (1997)
6. Rumianek, P., Dobosz, T., Nowak, R., Dziewit, P., and Aromiński, A. "Static mechanical properties of expanded polypropylene crushable foam". *Materials*, 14 (2021)
7. Sasso, M., Lattanzi, A., Farotti, E., Sarasini, F., Sergi, C., Tirillò, J., and Mancini, E. "Constitutive modelling of the dynamic behavior of cork material", Challenges in Mechanics of Time Dependent Materials, Mechanics of Biological Systems and Materials & Micro-and Nanomechanics, Volume 2. Conference Proceedings of the Society for Experimental Mechanics Series. Springer, Cham. https://doi.org/10.1007/978-3-030-86737-9_8, pages 57–63 (2022)
8. Mancini, E., Utzeri, M., Farotti, E., Lattanzi, A., and Sasso, M. "Dlp printed 3d gyroid structure: Mechanical response at meso and macro scale". *Mechanics of Materials*, 192:104970 (2024)
9. Sasso, M., Antonelli, M.G., Mancini, E., Radoni, M., and Amodio, D. "Experimental and numerical characterization of a polymeric hopkinson bar by dtma". *International Journal of Impact Engineering*, 103:50–63 (2017)
10. Martarelli, M., Mancini, E., Lonzi, B., and Sasso, M. "On the sensors calibration of polymeric hopkinson bars for dynamic testing of soft materials". *Measurement Science and Technology*, 29 (2018)
11. Utzeri, M., Sasso, M., Deshpande, V.S., and Kumar, S. "Multiscale experiments and predictive modeling for failure mitigation in additive manufacturing of lattices". *Advanced Materials Technologies*, 9 (24):2400457 (2024)
12. Kossa, A. and Berezvai, S. "Novel strategy for the hyperelastic parameter fitting procedure of polymer foam materials". *Polymer Testing*, 53:149–155 (2016)
13. *ANSYS Mechanical APDL Theory Reference*.
14. Ptak, M., Kaczynski, P., Fernandes, F., and de Sousa, R.A. "Assessing impact velocity and temperature effects on crashworthiness properties of cork material". *International Journal of Impact Engineering*, 106:238–248 (2017)
15. Zhang, M.G., Xu, W., Wu, T., Zhang, X.D., Zhang, H., Li, Z., Zhang, C., Jiang, H., and Chen, M. "Investigation on mullins effect of rubber materials by spherical indentation method". *Forces in Mechanics*, 4:100037 (2021)
16. Sasso, M., , Sarasini, F., Mancini, E., Lattanzi, A., Tirillò, J., and Sergi, C. "Experimental characterization and numerical modelling of the impact behavior of pvc foams". *Experimental Mechanics*, 63:823-837 (2023)